

1  
2  
3  
4  
5  
6  
7  
8  
9  
10  
11  
12  
13  
14  
15  
16  
17  
18  
19  
20  
21  
22

**Monitoring and modelling of soil-plant interactions:  
the joint use of ERT, sap flow and Eddy Covariance data  
to characterize the volume of an orange tree root zone.**

Giorgio Cassiani<sup>1</sup>, Jacopo Boaga<sup>1</sup>, Daniela Vanella<sup>2</sup>, Maria Teresa Perri<sup>1</sup>, Simona Consoli<sup>2</sup>

<sup>1</sup> University of Padua, Department of Geosciences, Italy

<sup>2</sup> University of Catania, Department of Agriculture, Food and Environment, Italy

**Re-submitted for publication to *HESS***

**March 2015**

23 **Abstract**

24 Mass and energy exchanges between soil, plants and atmosphere control a number of key  
25 environmental processes involving hydrology, biota and climate. The understanding of these  
26 exchanges also play a critical role for practical purposes e.g. in precision agriculture. In this paper  
27 we present a methodology based on coupling innovative data collection and models in order to  
28 obtain quantitative estimates of the key parameters of such complex flow system. In particular we  
29 propose the use of hydro-geophysical monitoring via “time-lapse” Electrical Resistivity  
30 Tomography (ERT) in conjunction with measurements of plant transpiration via sap flow and  
31 evapotranspiration from Eddy Covariance (EC). This abundance of data is fed to spatially  
32 distributed soil models in order to characterize the distribution of active roots. We conducted  
33 experiments in an orange orchard in Eastern Sicily (Italy), characterized by the typical  
34 Mediterranean semi-arid climate. The subsoil dynamics, particularly influenced by irrigation and  
35 root uptake, were characterized mainly by the ERT setup, consisting of 48 buried electrodes on 4  
36 instrumented micro boreholes (about 1.2 m deep) placed at the corners of a square (about 1.3 m in  
37 side) surrounding the orange tree, plus 24 mini-electrodes on the surface spaced 0.1 m on a square  
38 grid. During the monitoring, we collected repeated ERT and TDR soil moisture measurements, soil  
39 water sampling, sap flow measurements from the orange tree and EC data. We conducted a  
40 laboratory calibration of the soil electrical properties as a function of moisture content and pore  
41 water electrical conductivity. Irrigation, precipitation, sap flow and ET data are available allowing  
42 knowledge of the system’s long term forcing conditions on the system. This information was used  
43 to calibrate a 1D Richards’ equation model representing the dynamics of the volume monitored via  
44 3D ERT. Information on the soil hydraulic properties was collected from laboratory and field  
45 experiments. The successful results of the calibrated modelling exercise allow the quantification of  
46 the soil volume interested by root water uptake. This volume is much smaller (with a surface area

47 less than 2 square meters, and about 40 cm thickness) than expected and assumed in the design of  
48 classical drip irrigation schemes that prove to be losing at least half of the irrigated water which is  
49 not uptaken by the plants.

50 **Keywords:** Hydro-geophysics; Soil moisture; ERT, Eddy Covariance; Sap Flow; Root-zone.

51

## 52 **1. INTRODUCTION**

53 The system made of soil, vegetation and the adjacent atmosphere is characterized by complex  
54 patterns, structures, and processes that act on a wide range of time and space scales. While the  
55 exchange of energy and water is continuous between compartments, the pertinent fluxes are  
56 strongly heterogeneous and variable in space and time and this makes their quantification  
57 particularly challenging. Plants are known to impact the terrestrial water cycle and underground  
58 water dynamics through evapo-transpiration (ET) and root water uptake (RWU). The mechanisms  
59 of water flow in the root zone are controlled by soil physics, plant physiology and meteorological  
60 factors (Green et al., 2003a). The translation of plant water use strategies into physically-based  
61 models of root water uptake is a crucial issue in eco-hydrology and has fundamental consequence  
62 in the understanding and modelling of atmospheric as well as soil processes. Still, no consensus  
63 exists on the modelling of this process (Feddes et al., 2001; Raats, 2007). From a conceptual point  
64 of view, two main approaches exist today, which differ in the way of predicting the volumetric rate  
65 of RWU.

66 A first approach expresses water transport in plants as a chain process based on a resistance law.  
67 Coupled with a three-dimensional soil water flow model, this approach leads to fairly accurate  
68 RWU models at the plant scale (Doussan et al., 2006; Schneider et al., 2010), also under water  
69 stress conditions. The limitations of these models are the cost of characterizing parameters, such as  
70 root system architecture and conductance to water flow, and their computational demand. A second

71 approach, mostly used in soil-vegetation-atmosphere transfer models, relies on “macroscopic  
72 parameters” and predicts RWU as a product of the potential transpiration rate, a spatially  
73 distributed root parameter (e.g. relative root length density), and a stress function, depending on  
74 soil water potential and a compensatory RWU function (Jarvis, 1989). The major drawback of this  
75 approach is the necessity to calibrate the macroscopic parameters, which introduces substantial  
76 uncertainties (Musters and Bouten, 2000). Note that the two approaches have indeed some formal  
77 links with each other (Couvreur et al., 2012; Javaux et al., 2008).

78 The complexity of RWU modelling is highly related to the uneven root distribution in the vertical  
79 and radial directions (Gong et al., 2006). This variability is partly induced by heterogeneities in the  
80 soil and localized soil compaction caused by both cultivation and irrigation patterns (Jones and  
81 Tardieu, 1998) that in turn cause heterogeneous water and nutrient distribution. Consequently,  
82 there is a clear need for the development of novel RWU modelling approaches (Couvreur et al.,  
83 2012; Feddes et al., 2001; Raats, 2007; Jarvis, 2011;), as well as for accurate measurements  
84 techniques of soil water content and RWU dynamics.

85 In particular, soil moisture measurements are of paramount importance to calibrate RWU models.  
86 Traditionally, and especially beneath irrigated crops, soil moisture has been determined using  
87 methods such as neutron probes, TDR or capacitance systems. As these traditional techniques are  
88 point measurements, they do not provide sufficient information for reliable mass balance  
89 assessments; therefore our understanding of RWU as a spatially distributed system remains  
90 fundamentally limited. In this respect the understanding of soil as a spatially heterogeneous system  
91 shares fundamental limitations with most of earth sciences. Therefore much can be learnt looking  
92 at similar research fields.

93 Geophysical methods have long been established for the imaging of the soil subsurface at a variety  
94 of scales, from large scale mining exploration (e.g. Parasnis, 1973) to the very small scale of soil

95 mapping (e.g. Allred et al., 2008). The past twenty years, in particular, have seen the fast  
96 development of techniques that are useful in identifying structure and dynamics of the near surface,  
97 with particular reference to hydrological applications. This realm of research goes under the  
98 general name of hydro-geophysics (Binley et al., 201; Rubin and Hubbard, 2005, Vereecken et al.,  
99 2006) and covers a wide range of applications from flow and transport in aquifers (e.g. Kemna et  
100 al., 2002; Perri et al., 2012) to the vadose zone (e.g. Daily et al., 1992), from catchment (e.g. Weill  
101 et al., 2013) and hillslope characterization (Cassiani et al., 2009a) to agriculture and eco-  
102 hydrological processes (Boaga et al., 2014; Ursino et al., 2014).

103 Possibly the most interesting results have been obtained when hydro-geophysical data have been  
104 coupled with distributed hydrological model predictions. The degree of integration of data and  
105 model range from trial and error calibration (e.g. Binley et al., 2002) to full data assimilation (e.g.  
106 Hinnell et al., 2010), but in all cases the availability of spatially extensive (and time intensive) data  
107 greatly improve the models' capability to identify within narrow ranges the relevant governing  
108 parameters, that in turn are of practical interest for hydrological predictions.

109 Relatively few hydro-geophysical applications, though, have been focussed on plant root system  
110 characterization (e.g. al Hagrey et al, 2007; al Hagrey and Petersen, 2011; Javaux et al., 2008;  
111 Jayawickreme et al., 2008, Werban et al., 2008), often limiting the analysis to a tentative  
112 identification of the main root location and extent. Electrical soil properties are a clear indication  
113 of soil moisture content distribution and electrical and electromagnetic methods have been used to  
114 identify the effect of root activity (e.g. Cassiani et al., 2012; Shanahan et al., 2015). In particular,  
115 ERT has been used to characterize root water uptake and root system (Garré et al., 2011; Michot et  
116 al., 2001; Michot et al., 2003; Srayeddin and Doussan, 2009). Amato et al., (2009; 2010) tested the  
117 ability of 3D-ERT for quantifying root biomass on herbaceous plants. Beff et. al., (2013) used 3D-

118 ERT for monitoring soil water content in a maize field during late growing seasons. Boaga et al.,  
119 (2013) and Cassiani et al. (2015) demonstrated the reliability of the method in apple orchards.  
120 In this paper we aim at applying hydro-geophysical techniques, with a combination of  
121 measurements and modelling, to a tree root system. This approach has, to the best of our  
122 knowledge, not been presented and analysed yet. In particular, we present the application of the  
123 time-lapse non-invasive 3D electrical resistivity tomography (ERT) to monitor soil-plant  
124 interactions in the root zone of an orange tree located in the Mediterranean semi-arid Sicilian  
125 (South Italy) context. The subsoil dynamics, particularly influenced by irrigation and RWU, have  
126 been characterized by the 3D ERT measurements coupled with plant transpiration through sap flow  
127 measurements. The information contained in the ERT measurements in terms of vadose zone water  
128 dynamics was exploited by comparing the field results against a 1-D vadose zone model.

129 The specific goals of this paper are

- 130 (a) to study the feasibility of a small scale monitoring of root zone processes using time-lapse  
131 3D ERT;
- 132 (b) to assess the value of the data above for a quantitative description of hydrological processes  
133 at the tens of centimeter scale;
- 134 (c) to interpret these data with the aid of a physical hydrological model, in order to derive also  
135 information on the root zone physical structure and its dynamics.

136

## 137 **2. SITE DESCRIPTION**

138 The experiment was conducted in a 20-hectar orange orchard, planted with about 20 year-old trees  
139 (*Citrus sinensis*, cv Tarocco Ippolito) (Figure 1). The field is located in Lentini (Eastern Sicily, Lat.  
140 37°16'N, Long. 14°53'E) in a Mediterranean semi-arid environment, characterized by an annual  
141 average precipitation of around 550 mm, very dry summers and average air temperature of 7°C in

142 winter and 28°C in summer. The site presents conditions of crop homogeneity, flat slope, dominant  
143 wind speed direction for footprint analysis and quite large fetch that are ideal for  
144 micrometeorological measurements. The planting layout is 4.0 m × 5.5 m and the trees are drip  
145 irrigated with 4 in-line drippers per plant, spaced about 1 m, with 16 L h<sup>-1</sup> of total discharge (4 L h<sup>-1</sup>  
146 per dripper); the crop is well-watered by irrigation supplied every day from May to October, with  
147 irrigation timing of 5 h d<sup>-1</sup>. The study area has a mean leaf area index (LAI) of about 4 m<sup>2</sup> m<sup>-2</sup>,  
148 measured by a LAI-2000 digital analyser (LI-COR, Lincoln, Nebraska, USA). The LAI values are  
149 spatially averaged and are referred to the ERT measurement period (October 2013). In the specific  
150 case of a mature orange orchard, LAI values result fairly constant in time in the region of interest.

151 The mean PAR (photosynthetic active radiation) light interception was 80% within rows and 50%  
152 between rows; the canopy height ( $h_c$ ) is 3.7 m.

153 The soil characterization was performed via textural and hydraulic laboratory analyses, according  
154 to the USDA standards. The area, covered by mature orange orchards, was divided into regular  
155 grids, each having a 18 × 32 m<sup>2</sup> area, where undisturbed soil cores (0.05 m in height and 0.05 m in  
156 diameter) were collected at the 0-0.05 m and 0.05-0.10 m depths for a total of 32 sampling points  
157 and 64 soil samples. The undisturbed soil cores were used to determine the soil bulk density,  $\rho_b$   
158 (Mg m<sup>-3</sup>) and the initial water content,  $\theta_i$  (m<sup>3</sup> m<sup>-3</sup>), i.e. the  $\theta$  value at the time of the field campaign.  
159 A total of 32 disturbed soil samples were also collected at the 0-0.05 m depth to determine the soil  
160 textural characteristics using conventional methods following H<sub>2</sub>O<sub>2</sub> pre-treatment to eliminate  
161 organic matter and clay deflocculation using sodium metaphosphate and mechanical agitation (Gee  
162 and Bauder, 1986). Three textural fractions according to the USDA standards, i.e. clay (0-2  $\mu$ m),  
163 silt (2-50  $\mu$ m) and sand (50-2000  $\mu$ m), were used in the study to characterize the soil (Gee and

164 Bauder, 1986). Most soil textures (i.e. 27 out of 32) were loamy sand and the remaining textures  
165 were sandy loam.

166 An undisturbed soil sample was collected from the surface soil layer (0-0.05 m depth) at each  
167 sampling location (sample size,  $N = 32$ ), using stainless steel cylinders with an inner volume of  $10^{-4}$   
168  $\text{m}^3$  to determine the soil water retention curve. For each sample, the volumetric soil water content  
169 at 11 pressure heads,  $h$ , was determined by a sandbox ( $h = 0.01, 0.025, 0.1, 0.32, 0.63, 1.0$  m) and a  
170 pressure plate apparatus ( $h = 3, 10, 30, 60, 150$  m). For each sample, the parameters of the van  
171 Genuchten (1980, vG) model for the water retention curve with the Burdine (1953) condition were  
172 determined (Aiello et al., 2014).

173 Three soil water content profiles are measured in the field using water content reflectometers  
174 (TDR, Time Domain Reflectometry), since 2009. Calibrated Campbell Scientific CS616 water  
175 content reflectometers ( $\pm 2.5\%$  of accuracy) were installed to monitor every 1 h the changes of  
176 volumetric soil water content ( $\Delta\theta$ ). The TDR probe installation was designed to measure soil water  
177 content variations with time in the soil volume afferent to each plant. The TDR probes location is  
178 considered well suited with the specific characteristics of the micro-irrigation systems used in the  
179 area and the textural soil main features. For each location the TDR equipment consists of two  
180 sensors inserted vertically at 0.20 and 0.45 m depth and of two sensors inserted horizontally at 0.35  
181 m depth, with 0.20 m in between. The water content reflectometer consists of two stainless steel  
182 rods connected to a printed circuit board. When the probe rods were inserted vertically into the soil  
183 surface they gave an indication of the water content in the upper 20-25 cm of soil. The probes  
184 installed horizontal to the surface were used to detect the passing of wetting fronts of water fluxes.

185 The data that are discussed here (see results section) correspond to the TDR probes located at  
186 about 1.5 m from the orange tree we monitored with ERT.



187 Hourly meteorological data (incoming short-wave solar radiation, air temperature, air humidity,  
188 wind speed and rainfall) are acquired by an automatic weather station located about 7 km from the  
189 orchard and managed by SIAS (Agro-meteorological Service of the Sicilian Region). For the  
190 dominant wind directions, the fetch is larger than 550 m. For the other sectors the minimum fetch  
191 is 400 m (SE).

### 192 **3. METHODOLOGY**

#### 193 *3.1 Micrometeorological measurements*

194 The experimental site is equipped with Eddy Covariance (EC) systems mounted on a  
195 micrometeorological fluxes tower (Figure 1). Continuous energy balance measurements have been  
196 since 2009. In particular, net radiation ( $R_n$ ,  $W m^{-2}$ ) is measured with two CNR 1 Kipp&Zonen  
197 (Campbell Scientific Ltd) net radiometers at a height of 8 m. Soil heat flux density ( $G$ ,  $W m^{-2}$ ) is  
198 measured with three soil heat flux plates (HFP01, Campbell Scientific Ltd) placed horizontally  
199 0.05 m below the soil surface. Three different measurements of  $G$  were selected: in the trunk row  
200 (shaded area), at 1/3 of the distance to the adjacent row, and at 2/3 of the distance to the adjacent  
201 row. The soil heat flux is measured as the mean output of three soil heat flux plates. Data from the  
202 soil heat flux plates is corrected for heat storage in the soil above the plates.

203 The air temperature and the three wind speed components are measured at two heights, 4 and 8 m,  
204 using fine wire thermocouples (76  $\mu m$  diameter) and sonic anemometers (Windmaster Pro, Gill  
205 Instruments Ltd, at 4m, and a CSAT, Campbell Sci., at 8 m). A gas analyzer (LI-7500, LI-COR)  
206 operating at 10 Hz was installed at 8 m. The raw data are recorded at a frequency of 10 Hz using  
207 two synchronized data loggers (CR3000, Campbell Sci.).

208 The Eddy Covariance measurement system and the data processing followed the guidelines of the  
209 standard EUROFLUX rules (Aubinet et al., 2000). A data quality check was applied during the

210 post processing together with some routines to remove the common errors: running means for de-  
211 trending, three angle coordinate rotations and de-spiking. Stationarity and surface energy closure  
212 were also checked (Kaimal and Finnigan, 1994).

213 Low frequency measurements are taken for air temperature and humidity (HMP45C, Vaisala),  
214 wind speed and direction (05103 RM Young), and atmospheric pressure (CS106, Campbell  
215 Scientific Ltd) at 4, 8 and 10 m.

216 The freely distributed TK2 package (Mauder and Foken, 2004) is used to determine the first and  
217 second order statistical moments and fluxes on a half-hourly basis following the protocol used as a  
218 comparison reference described in Mauder et al. (2007).

### 219 *3.2 Sap flow measurements*

220 Heat-pulse techniques can be used to measure sap flow in plant stems with minimal disruption to  
221 the sap stream (Cohen et al., 1981; Green and Clothier, 1988; Swanson and Whitfield, 1981). The  
222 measurements are reliable, use inexpensive technology, provide a good time resolution of sap flow,  
223 and they are well-suited to automatic data collection and storage. Sequential or simultaneous  
224 measurements on numerous trees are possible, permitting the estimation of transpiration from  
225 whole stands of trees.

226 Measurements of water consumption at tree level ( $T_{SF}$ ) have been taken using the HPV (Heat Pulse  
227 Velocity) technique that is based on the measurement of temperature variations ( $\Delta T$ ), produced by  
228 a heat pulse of short duration (1-2 s), in two temperature probes installed asymmetrically on either  
229 side of a linear heater that is inserted into the trunk. For HPV measurements, two 4 cm sap flow  
230 probe with 4 thermocouples embedded (Tranzflo NZ Ltd., Palmerston North, NZ) were inserted in  
231 the trunks of the trees, belonging to the area of footprint of the micrometeorological eddy  
232 covariance tower. The probes were positioned at the North and South sides of the trunk at 50 cm

233 from the ground and wired to a data-logger (CR1000, Campbell Sci., USA) for heat-pulse control  
234 and measurement; the sampling interval was 30 min. The temperature measurements are obtained  
235 by means of ultra-thin thermocouples that, once the probes are in place, are located at 5, 15, 25 and  
236 45 mm within the trunk.

237 Data have been processed according to Green et al. (2003b) to integrate sap flow velocity over  
238 sapwood area and calculate transpiration. In particular, the volume of sap flow ( $Q_{\text{stem}}$ ) in the tree  
239 stem is estimated by multiplying the sap flow velocity by the cross sectional area of the conducting  
240 tissue. To this purpose, fractions of wood ( $F_M=0.48$ ) and water ( $F_L=0.33$ ) in the sapwood were  
241 determined on the trees where sap flow probes were installed. Wound-effect correction (Consoli  
242 and Papa, 2013; Green et al., 2003b; Motisi et al., 2012) was done on a per-tree basis. Crop  
243 transpiration data are available at the study site since 2009.

### 244 ***3.3 Electrical resistivity tomography (ERT)***

245 The key technique used to monitor the soil moisture content distribution in the volume surrounding  
246 the orange tree is electrical resistivity tomography (ERT – e.g. Binley and Kemna, 2005). In  
247 particular, we installed a three-dimensional ERT system, consisting of 48 buried electrodes placed  
248 on 4 instrumented micro-boreholes, with 12 electrodes each (see Figure 2). The electrodes are  
249 made of stainless steel wound around a one-inch PVC pipe, and are spaced 10 cm along the pipe  
250 (see inset in Figure 2), thus the shallowest and the deepest are respectively at 0.1 m and 1.2 m  
251 below the surface. Each electrode is made of a plate 3 cm wide. The boreholes are placed at the  
252 vertices of a square, having a side of 1.3 m, that has the orange tree at its centre, and were inserted  
253 by percussion with the help of a pre-drilling with a smaller diameter in order to avoiding the  
254 disturbance of the electrical flow. The electrical contact is excellent for all 48 buried electrodes, as  
255 checked before each measurement. The 4 boreholes are water tight and in tight contact with the

256 soil, so they cannot act as pathways for preferential water infiltration. We focused our attention to  
257 an area slightly smaller than the square defined by the boreholes, in order to avoid the inevitable  
258 disturbance caused by borehole installation (slightly compacting the surrounding soil). The system  
259 is completed by 24 electrodes at the ground surface, placed along a square grid of about 0.21 m  
260 side, covering the 1.3 m x 1.3 m square at the surface (Figure 3): this setup allows a homogeneous  
261 coverage of the surface of the control volume. The chosen acquisition scheme was a skip-zero  
262 dipole-dipole configuration, i.e. a configuration where the current dipoles and potential dipoles are  
263 both of minimal size, i.e. they consist of neighbouring electrodes e.g. along the boreholes. This  
264 setup ensures maximal spatial resolution (as good as the electrode spacing, at least close to  
265 electrodes themselves) provided that the signal/noise ratio is sufficiently high. The data quality is  
266 assessed using a full acquisition of reciprocals to estimate the data error level (see e.g., Binley et  
267 al., 1995; Monego et al., 2010). Consistently, we used for the 3D data inversion an Occam  
268 approach as implemented in the R3 software package (Binley, 2014) accounting for the error level  
269 estimated from the data themselves. The relevant three-dimensional computational mesh is shown  
270 in Figure 3. At each time step, about 90-95 % of the dipoles survived the 10% reciprocal error  
271 threshold. In order to build a time-consistent data set, only the dipoles surviving this error analysis  
272 for all time steps were subsequently used, reducing the number to slightly over 90% of the total.  
273 The absolute inversions were run using the same 10% error level. Time-lapse inversions were run  
274 at a lower error level equal to 2 % (consistently with the literature – e.g., Cassiani et al., 2006).

275 We conducted repeated ERT measurements using the above apparatus for about two days, starting  
276 on October 2, 2013 at 11:00 am, and ending the next day at about 16:00. The schedule of the  
277 acquisitions and the irrigation times is reported in Table 1. Note that the background ERT survey  
278 was acquired on October 2 at 11:00 before the first irrigation period was started, so that all changes  
279 caused by irrigation and subsequent evapotranspiration can be referred to that instant. Note that

280 prior to October 2, 2013, irrigation had been suspended for at least 15 days. Note also that only one  
281 dripper – with a flow of about 4 l/h – is located at the surface of the control volume defined by the  
282 ERT setup (Figure 3).

283

#### 284 **4. RESULTS AND DISCUSSION**

285 The paper presents results derived from both short term (2 days) and long term monitoring. The  
286 micrometeorological data set (including the measurements of the energy balance components) and  
287 the sap flow data are available since 2009. ERT measurements were carried out only during a 2-  
288 day period, but the state of the system at the time of the ERT measurements clearly depends on the  
289 past forcing acting on the system. In order to fully exploit the information content of this dataset,  
290 we aimed at comparing data against simulations, as much as possible in a quantitative manner.

291 The ERT monitoring as described in Table 1 produced two clear results:

292 (1) The initial conditions (11:00 a.m. of October 2, before irrigation starts) around the tree  
293 show a very clear difference in electrical resistivity in the top 40 cm of soil with respect to  
294 the rest of the volume (Figure 4). Specifically, the resistivity of the top layer ranges around  
295 40-50 Ohm m, while the lower part of the profile is about one order of magnitude more  
296 conductive (about 5 Ohm m). As no apparent lithological difference is present at 40 cm  
297 depth (see also laboratory results below) we attributed this difference to a marked  
298 difference in soil moisture content. This was confirmed by all following evidence (see  
299 below).

300 (2) The resistivity changes as a function of time, during the two irrigation periods, during the  
301 night interval, and afterwards, all show essentially the same pattern, with relatively small  
302 (but still clearly measurable) changes (Figure 5). Two zone are identifiable: (a) a shallow

303 zone (top 10-20 cm) where resistivity decreases with respect to the initial condition; and (b)  
304 a deeper zone (20-40 cm) where resistivity increases.

305 Qualitatively, both pieces of evidence can be easily explained in terms of water dynamics governed  
306 by precipitation, irrigation and root water uptake. Specifically, the shallower high resistivity zone  
307 in Figure 4 can be correlated to a dry region where root water uptake manages to keep soil moisture  
308 content to minimal values, as an effect of the entire summer strong transpiration drive. The  
309 dynamics in Figure 5, albeit small compared to the initial root uptake signal in Figure 4, still  
310 confirm that the top 40 cm is house to a strong root activity, to the point that irrigation cannot raise  
311 electrical conductivity of the shallow zone (10-20 cm) by no more than some 20%, and the roots  
312 manage to make the soil even drier (with a resistivity increase by some 10%) in the 20-40 cm depth  
313 layer (Figure 5). Note that, in general, resistivity changes of the type here observed cannot be  
314 uniquely associated to soil moisture content changes, as pore water conductivity may play a key  
315 role (e.g. Boaga et al., 2013; Ursino et al., 2014). However, in the particular case at hand, care was  
316 taken to analyze the electrical conductivity of both the water used for irrigation and the pore water,  
317 purposely extracted at about 50 cm depth. Both waters showed an electrical conductivity value in  
318 the range of 1300  $\mu\text{S}/\text{cm}$  (thus fairly high, fact that explains the overall small soil resistivity  
319 observed at the site). Therefore in this particular case we can exclude pore water conductivity  
320 effects in the observed dynamics of the system. Once again it must be stressed that this is rather the  
321 exception than the rule.

322 A laboratory-based method was adopted for obtaining “unaltered” soil pore water through a  
323 column displacement technique (Knight et al., 1998). In particular, Rhizon soil moisture samplers  
324 (Cabrera, 1998) were used; they represent one of the latest developments in terms of tension  
325 samplers, where it is necessary to apply a suction to withdraw pore water with a vacuum tube (Tye  
326 et al., 2003). .

327 The qualitative evidence above is, however, not very surprising and not particularly informative:  
328 the root activity dries the soil, this is not a discovery. Things become more interesting if we can  
329 translate the ERT data into quantitative estimates of soil moisture content, and if we can use these  
330 data to calibrate hydrological models of the root zone.

331 To this end, we tested Bulgherano soil samples in the laboratory to obtain a suitable constitutive  
332 relationship linking moisture content and resistivity, given the known pore water conductivity that  
333 was reproduced for the water used in the laboratory. All measurements were conducted using  
334 cylindrical Plexiglas cells equipped with a four-electrode configuration designed to allow for  
335 sample saturation and de-saturation with no sample disturbance, using an air injection apparatus at  
336 one end and a ceramic plate at the opposite end. The air entry pressure of the ceramic  
337 is 1 bar, thus during all the experiments the plate remained under full water saturation,  
338 while allowing water outflow during de-saturation. At each de-saturation step, the electrical  
339 conductivity of the sample was measured under temperature controlled conditions using a ZEL-  
340 SIP04 impedance meter (Zimmermann et al. 2008). A completed description of the setup is  
341 given by Cassiani et al. (2009b).

342 Figure 6 shows two example experimental results on samples from two different depths. Note how  
343 in a wide range of soil moisture content (roughly from 5% to saturation) the two curves in Figure 6  
344 lie practically on top of each other. The same applies for all tested samples. Note also that, even  
345 though some samples show the effect of the conductivity of the solid phase (through its clay  
346 fraction) at small saturation (see sample from 0.4 m in Figure 6) still the effect is small as it  
347 appears only at soil moisture smaller than 3-4%. Therefore we deemed unnecessary to resort to  
348 constitutive laws that represent this solid phase effect, such as Waxman and Smits (1968) that has  
349 been used for similar purposes elsewhere (e.g. Cassiani et al., 2012) and we adopted a simpler  
350 Archie's (1942) formulation. Consequently we translated resistivity into moisture content using the

351 following relationship calibrated on the laboratory data, using a water having the above mentioned  
352 electrical conductivity:

$$353 \quad \theta = \frac{4.703}{\rho^{1.12}} \quad (1)$$

354 where  $\theta$  is volumetric soil moisture content (dimensionless) and  $\rho$  is electrical resistivity (in Ohm  
355 m). The relationship (1) allows a direct translation of the 3D resistivity distribution to a  
356 corresponding distribution of volumetric soil moisture content. However, it has long been  
357 established that inverted geophysical data may bring with them enough distortion of the true  
358 physical parameter field (Day-Lewis et al., 2005) as to induce violations of elementary physical  
359 principles, such as mass balance during tracer test monitoring experiments (e.g. Singha and  
360 Gorelick, 2005). This may cause substantial problems, particular when the use of data is expected  
361 to shift from a qualitative interpretation to a quantitative use in terms of data assimilation into  
362 hydrological models. For this reason, coupled versus uncoupled approaches have been proposed  
363 and discussed (Hinnell et al., 2010) even though their superiority seems to depend on the specific  
364 problem, as the information content of data even in a tradition, inverted approach may be sufficient  
365 (Camporese et al., 2011, 2014). Indeed, the geometry we are considering here is very effective to  
366 reconstruct the mass balance of irrigated water, as this comes as a quasi-one dimensional  
367 infiltration front from the top, where in addition electrodes are located. The geometry is similar to  
368 the one used, e.g., Koestel et al. (2008) where mass balance was verified by comparison against  
369 very detailed TDR data collected in a lysimeter. In spite of these considerations, we decided to still  
370 limit ourselves to analyzing the data variation principally as a function of depth, lumping the data  
371 horizontally by averaging estimated moisture content along two-dimensional horizontal planes.  
372 Note that the dataset may lend itself to more complex analyses such as the one proposed by Manoli  
373 et al. (2014), especially if used in the context of a formal Data Assimilation, but we felt that one



374 such an endeavor would exceed the scope of the current paper and deserves an ad-hoc space. Note  
375 also that the ERT field evidence both in terms of background (Figure 4) and time-lapse evolution  
376 (Figure 5) of moisture content confirm the hypothesis that, within the control volume, the  
377 distribution of water in the soil is largely one-dimensional as a function of depth.

378 The data, once condensed in this manner, lend themselves more easily to a comparison with the  
379 results of infiltration modeling. We implemented a one-dimensional finite element model based on  
380 a Richards' equation solver (*Femwater* – details of this classical model are given by Lin et al.,  
381 1997), simulating the central square meter of the ERT monitored control volume, down to a total  
382 depth of 2 meters (much below the depth of the ERT boreholes), where we assumed that the water  
383 table is located (Dirichlet boundary condition). We applied at the top of the soil column a  
384 Neumann boundary condition consistent with the flux coming from irrigation that pertains the  
385 control volume (basically, the water coming from a single dripper). As *Femwater* is a 3D simulator,  
386 the soil column is also bounded laterally by no-flow conditions, with the exception of the top 40  
387 cm where we applied laterally a Neumann condition simulating the root water uptake (see below  
388 for details).

389 We considered only the central part of the ERT-controlled volume (1 m x 1 m) thus excluding the  
390 regions too close to the boreholes that, even though benefitting from the best ERT sensitivity,  
391 might have been altered from a hydraulic viewpoint by the drilling and installing operations.  
392 Correspondingly we averaged horizontally the ERT data only in this central region.

393 A very fine vertical discretization (0.01 m) and time stepping (0.01 h) ensures solution stability.  
394 The porous medium is homogeneous along the column and parameterized according to the Van  
395 Genuchten (1980) model. The relevant parameters had been derived independently from laboratory  
396 and field measurements, the latter particularly relevant for the definition of a reliable in situ  
397 saturated hydraulic conductivity estimate. The parameters used for the simulations are: residual

398 moisture content  $\theta_r = 0.$ , porosity  $\theta_s=0.54$ ,  $\alpha = 0.12$  1/m,  $n = 1.6$ , saturated hydraulic conductivity  
399  $K_s = 0.002$  m/h. We acknowledge that a more complete sensitivity analysis concerning the impact  
400 of the individual parameters would be beneficial, but this should be performed in a complete Monte  
401 Carlo manner in order to exclude identification trade-offs between the Van Genuchten parameters,  
402 the depth of the water table (known with some uncertainty) and the fluxes from irrigation,  
403 precipitation and evapotranspiration. However we feel that this endeavour shall be conducted also  
404 with regard to the effective 3D spatial distribution of active roots, and is currently the subject of  
405 ongoing research.

406 The remaining elements of the predictive modelling exercise are initial and boundary conditions.  
407 As we focused primarily our attention on reproducing the state of the system at background  
408 conditions, we set the start of the simulation at the beginning of the year (1/1/2013), and we  
409 assumed for that time a condition drained to equilibrium. Given the van Genuchten parameters we  
410 used and the depth of the water table, this corresponds to a fairly wet initial condition. We verified  
411 a posteriori that moving the initial time back of one or more years did not alter the predicted results  
412 at the date of interest (October 3, 2013). The dynamics during the year are sufficient to bring the  
413 system to the real, much drier condition in October. The forcing conditions on the system are all  
414 known: (a) irrigation is recorded, and only one dripper pertains to the considered square meter; (b)  
415 precipitation is measured; (c) sap flow is measured. Direct evaporation from the square meter of  
416 soil around the stem is neglected, considering the dense canopy cover and the consequent limited  
417 radiation received. Only one degree of freedom is left to be calibrated, i.e. the volume from which  
418 the roots uptake water. Thickness of the active root zone was estimated from the time-lapse  
419 observations (Figure 5), and fixed to the top 0.4 cm after checking that limiting the root uptake to  
420 the 0.2 m to 0.4 m zone would produce results inconsistent with observations in the top 0.2 m.  
421 Therefore only the surface area of the root uptake zone remains to be estimated. We used the

422 predictive model as a tool to identify the extent of this zone, that is of critical interest also for  
423 irrigation purposes.

424 Figure 7 shows the results of the calibration exercise. It is apparent that the total areal extent of the  
425 root uptake zone has a dramatic impact on the predicted moisture content profiles, as it scales the  
426 amount of water subtracted from the monitored square meter considered in the calibration. Even  
427 relatively small changes (+/-15%) of the root uptake area produce very different soil moisture  
428 profiles. The value that allows a good match of the observed profile is  $1.75 \text{ m}^2$ , while for areas  
429 equal to  $1.5 \text{ m}^2$  and  $2 \text{ m}^2$  the match is already unsatisfactory, leading respectively to  
430 underestimation and overestimation of the moisture content in the profile.

431 Another important fact that is apparent from Figure 7 is that the estimated soil moisture in the  
432 shallow zone (roughly down to 0.4 m) is very small as an effect of root water uptake. However this  
433 dry zone must have a limited areal extent ( $1.75 \text{ m}^2$ , corresponding to a radius of about 0.75 m from  
434 the stem of the tree). Indeed this is indirectly confirmed by the soil moisture evolution measured by  
435 TDR. Figure 8 shows the TDR data from three probes located about 1.5 m from the monitored tree  
436 (thus outside our estimated root uptake zone). The signal coming from the irrigation experiment of  
437 October 2, 2013 is very apparent with an increase in moisture content of all three probes, located at  
438 different depths. Note that before this experiment the system had been left without irrigation for  
439 about two weeks. The corresponding effect on the TDR data is apparent: all three probes show a  
440 decline of moisture content during the day, with pauses overnight. The decline is more pronounced  
441 in the 0.35 m TDR probe, that lies at a depth we estimated to be nearly at the bottom of the RWU  
442 zone, and less pronounced above (0.2 m) and below (0.45 m). Note also that the TDR probes are  
443 close to another dripper, lying outside of the ERT controlled volume (the drippers are spaced 1 m  
444 along the orange trees line, with the trees about 4 m from each other) thus they reflect directly the  
445 infiltration from that dripper. However, at all three depths the moisture content is much higher than

446 measured in the ERT-controlled block closer to the tree. This can be explained with the fact that in  
447 that region the root uptake is minimal or totally absent, while the decline of moisture content in  
448 time may well be an effect of water being drawn to the root zone by lateral movement induced by  
449 the very strong capillary forces exerted by the dry fine grained soil in the active root zone closer to  
450 the tree. In order to clarify the impact of these results on our understanding of the system, we show  
451 the location of the trees, of the TDR probes and of the drippers in Figure 9, where we also sketch  
452 the best estimate for the areal extent of the RWU zone. This Figure clearly highlights how critical  
453 the information provided by ERT actually is. The scale at which RWU takes place is smaller  
454 (meter scale) than expected and often assumed when it comes to designing and implementing a  
455 field monitoring system. This has dramatic consequences in terms of how reliable conclusions can  
456 be drawn if such a small scale processes are neglected. Consider, e.g., what type of conclusions  
457 could be drawn on the basis of TDR data alone (Figure 8) in light of the field situation as depicted  
458 in Figure 9. The single, most important message that shall be conveyed by this paper is a warning  
459 to be particularly attentive to small scale processes in soil-plant-atmosphere interactions, even in  
460 regular agricultural landscapes.

461

## 462 **5. CONCLUSIONS**

463 Near surface geophysics is strongly affected by both static and dynamic soil/subsoil characteristics.  
464 This fact, if properly recognized, is potentially full of information on the soil/subsoil structure and  
465 behaviour. The information is maximized if geophysical data are collected in time-lapse mode. In  
466 the case of interactions with vegetation, its role should be properly modelled, and such models can  
467 be constrained by means (also) of geophysical data. This case study demonstrates that 3D ERT is  
468 capable of characterizing the pathways of water distribution, and provides spatial information on  
469 root zone suction regions. The integration of modelling and data has proven, once again, a key

470 component of this type of hydro-geophysical studies, allowing us to draw quantitative results of  
471 practical interest. In this case we had available a wealth of quantitative information about  
472 transpiration and soil moisture content that allowed the definition of the volume of soil affected  
473 by the RWU activity. This has obvious consequences for the possible improvement of irrigation  
474 strategies, as it is apparent how the monitored orange tree essentially drives water from 1 to 2  
475 drippers out of the 4 total that should pertain to its area in the plantation. This means that it is very  
476 likely that half of the irrigated water is indeed lost to deeper layers and brings no contribution to  
477 the plants. More advanced uses of this type of data are now considered, especially linking soil  
478 moisture distribution with plant physiological response and active root distribution in the soil. In  
479 the long run studies of this type may give a fundamental contribution to our understanding of soil-  
480 plant-atmosphere interactions also in view of facing challenges coming from climatic changes.

481

## 482 **6. ACKNOWLEDGEMENTS**

483 We wish to acknowledge support from the EU FP7 project GLOBAQUA (“Managing the effects of  
484 multiple stressors on aquatic ecosystems under water scarcity”) and the MIUR PRIN project  
485 2010JHF437 “Innovative methods for water resources management under hydro-climatic  
486 uncertainty scenarios”. We also wish to thank the Agro-meteorological Service of the Sicilian  
487 Region for supporting field campaigns.

488

489

490 **7. REFERENCES**

- 491 Aiello, R., Bagarello, V., Barbagallo, S., Consoli, S. Di Prima, S., Giordano, G., Iovino, M., 2014,  
492 An assessment of the Beerkan method for determining the hydraulic properties of a sandy  
493 loam soil. *Geoderma*, 235–236 (2014) 300–307
- 494 al Hagrey S. A., 2007, Geophysical imaging of root-zone, trunk, and moisture heterogeneity, *J.*  
495 *Exp. Bot.*, 58, 839 – 854.
- 496 al Hagrey SA, Petersen T. Numerical and experimental mapping of small root zones using  
497 optimized surface and borehole resistivity tomography. *Geophysics* 2011;76(2):doi:  
498 10.1190/1.3545067.671
- 499 Allred B., Daniels, J.J. and Reza Ehsani, M., 2008, *Handbook of Agricultural Geophysics*, CRC  
500 Press, 432 pp.
- 501 Amato, M., Rossi, R., Bitella, G., Lovelli, S., 2010, Multielectrode Geoelectrical Tomography for  
502 the Quantification of Plant Roots. *Ital. J. Agron. / Riv. Agron.*, 3:257-263.
- 503 Amato, M., Bitella, G., Rossi, R., Gomez, J. A., Lovelli, S. and Gomes J. J. F., 2009, Multi-  
504 electrode 3D resistivity imaging of alfalfa root zone,” *European Journal of Agronomy*, vol. 31,  
505 no. 4, pp. 213–222.
- 506 Archie, G.E. 1942. The electrical resistivity log as an aid in determining some reservoir  
507 characteristics. *Trans. AIME* 146:54–67.
- 508 Aubinet, M, Grelle, A, Ibrom, A, Rannik, U, Moncrieff, J., Foken, T., Kowalski, P., Martin, P.,  
509 Berbigier, P., Bernhofer, C., Clement, R., Elbers, J., Granier, A., Grunwald, T., Morgenster,  
510 K., Pilegaard, K., Rebmann, C., Snijders, W., Valentini, R., Vesala, T., 2000, Estimates of the  
511 annual net carbon and water exchange of European forests: the EUROFLUX methodology,  
512 *Adv.Ecol.Res.* 30: 113-75.

513 Beff., L., Gunther, T., Vandoorne, B., Couvreur, V., Javaux, M., 2013, Three-dimensional  
514 monitoring of soil water content in a maize field. *Hydrol. Earth Syst. Sci.*, 17, 595–609.  
515 doi:10.5194/hess-17-595-2013 using Electrical Resistivity Tomography.

516 Binley A.M. and Kemna, A., 2005, DC resistivity and induced polarization methods. In: Rubin Y,  
517 Hubbard SS (eds) *Hydrogeophysics*. Water Sci. Technol. Library, Ser. 50. Springer, New  
518 York, pp 129–156

519 Binley, A., Ramirez, A., Daily, W. (1995) Regularised image reconstruction of noisy electrical  
520 resistance tomography data. In: Beck MS, Hoyle BS, Morris MA, Waterfall RC, Williams RA  
521 (eds), *Process tomography*. Proceedings of the 4th Workshop of the European Concerted  
522 Action on Process Tomography, Bergen, 6–8, April 1995, pp. 401– 410.

523 Binley, A., 2014, <http://www.es.lancs.ac.uk/people/amb/Freeware/freeware.htm> (last access: August  
524 2014).

525 Binley A.M, Cassiani, G. and Deiana, R., 2011, *Hydrogeophysics – Opportunities and Challenges*,  
526 *Bollettino di Geofisica Teorica ed Applicata*, 51(4), 267-284.

527 Binley A.M., Cassiani G., Middleton R., Winship P., 2002, Vadose zone flow model  
528 parameterisation using cross-borehole radar and resistivity imaging, *Journal of Hydrology*;  
529 267:147-159.

530 Boaga J., Rossi M., and Cassiani, G., 2013, Monitoring soil-plant interactions in an apple orchard  
531 using 3D electrical resistivity tomography, *Conference on Four Decades of Progress in*  
532 *Monitoring and Modeling of Processes in the Soil-Plant-Atmosphere System: Applications and*  
533 *Challenges*, Naples, 19-21 June 2013; Series: *Procedia Environmental Sciences* Volume: 19  
534 Pages: 394-402.

535 Boaga J., D'Alpaos, A., Cassiani, G., Marani, M., Putti, M., 2014, Plant-soil interactions in salt-  
536 marsh environments: experimental evidence from electrical resistivity tomography (ERT) in  
537 the Venice lagoon, in press, *Geophysical Research Letters*.

538 Burdine, N.T., 1953, Relative permeability calculation from pore size distribution data. *Trans. Am.*  
539 *Inst. Min. Eng.*, 198, 71-78.

540 Cabrera, R.I., (1998), Monitoring chemical properties of container growing media with small soil  
541 solution samplers. *Scientia Horticulturae*, 75, 113-119.

542 Camporese M., Salandin, P., Cassiani G., and Deiana, R., 2011, Impact of ERT data inversion  
543 uncertainty on the assessment of local hydraulic properties from tracer test experiments, *Water*  
544 *Resources Research*, 47, W12508, doi:10.1029/2011WR010528.

545 Camporese M., Cassiani, G., Deiana, R., Salandin, P., Binley, A. M., 2014, Comparing coupled  
546 and uncoupled hydrogeophysical inversions using ensemble Kalman filter assimilation of  
547 ERT-monitored tracer test data, submitted, *Water Resources Research*.

548 Cassiani, G., Bruno, V., Villa, A., Fusi, N., and Binley, A. M., 2006, A saline trace test monitored  
549 via time-lapse surface electrical resistivity tomography, *J. Appl. Geophys.*, 59, 244–259.

550 Cassiani G., Godio, A., Stocco, S., Villa, A., Deiana, R., Frattini, P., Rossi, M., 2009a, Monitoring  
551 the hydrologic behaviour of steep slopes via time-lapse electrical resistivity tomography, *Near*  
552 *Surface Geophysics*, special issue on Hydrogeophysics – Methods and Processes, p.475-486,  
553 doi: 10.3997/1873-0604.2009013. Cassiani, G., A. Kemna, A. Villa, and E. Zimmermann,  
554 2009b, Spectral induced polarization for the characterization of free-phase hydrocarbon  
555 contamination in sediments with low clay content, *Near Surface Geophysics*, special issue on  
556 Hydrogeophysics – Methods and Processes, p. 547-562. doi: 10.3997/1873-0604.2009028.

557 Cassiani G., Ursino, N., Deiana, R., Vignoli, G., Boaga, J., Rossi, M., Perri, M. T., Blaschek, M.,  
558 Duttman, R., Meyer, S., Ludwig, R., Soddu, A., Dietrich, P. and Werban, U., 2012, Non-



559 invasive monitoring of soil static characteristics and dynamic states: a case study highlighting  
560 vegetation effects, *Vadose Zone Journal*, Special Issue on SPAC - Soil-plant interactions from  
561 local to landscape scale, August 2012, V.11, vzj2011.0195, doi: 10.2136/2011.0195.

562 Cassiani G., J. Boaga, M. Rossi, G. Fadda, M. Putti, B. Majone, A. Bellin, 2011, Soil-plant  
563 interaction monitoring: small scale example of an apple orchard in Trentino, North-Eastern  
564 Italy, *in press*, *Science of the Total Environment*.

565 Cohen, Y., Fuchs, M., and Green, G.C., 1981, Improvement of the heat-pulse method for  
566 determining sap flow in trees. *Plant Cell Environ.* 4:391–397.

567 Consoli, S., Papa, R., 2013, Corrected surface energy balance to measure and model the  
568 evapotranspiration of irrigated orange orchards in semi-arid Mediterranean conditions.  
569 *Irrigation Science* September 2013, Volume 31, , pp 1159-1171

570 Couvreur, V., Vanderborght, J., Javaux, M., 2012, A simple three-dimensional macroscopic root  
571 water uptake model based on the hydraulic architecture approach. *Hydrol. Earth Syst. Sci.*, 16,  
572 2957–2971. doi:10.5194/hess-16-2957-2012

573 Daily W., Ramirez, A., LaBrecque, D., Nitao, J., 1992, Electrical resistivity tomography of vadose  
574 zone movement, *Water Resources Research*, 28(5), 1429-1442.

575 Day-Lewis, F.D., Singha, K., Binley, A.M.; 2005, Applying petrophysical models to radar travel  
576 time and electrical resistivity tomograms: Resolution-dependent limitations. *Journal of*  
577 *Geophysical Research-Solid Earth*, 110 (B8), B08206.

578 Doussan, C ., Pierret, A., Garrigues, E., Pagès, L., 2006, Water uptake by plant roots: II –  
579 Modelling of water transfer in the soil root-system with explicit account of flow within the root  
580 system –Comparison with experiments. *Plant and Soil* 283:99–117. DOI 10.1007/s11104-004-  
581 7904-z.

582 Feddes, R. A., Hoff, H., Bruen, M., Dawson, T., de Rosnay, P., Dirmeyer, P., Jackson, R. B.,  
583 Kabat, P., Kleidon, A., Lilly, A., Pitman, A. J., 2001, Modelling Root Water Uptake in  
584 Hydrological and Climate Models. Bulletin of the American Meteorological Society, Vol. 82,  
585 No. 12, 2797-2809.

586 Garré, S., Javaux, M., Vanderborght, J., Pagès, L., Vereecken, H., 2011, Three-Dimensional  
587 Electrical Resistivity Tomography to Monitor Root Zone Water Dynamics. Vadose Zone  
588 Journal 10(1):412-424. DOI: 10.2136/vzj2010.0079.

589 Gee, GW and Bauder. JW, 1986, Particle-size analysis. p. 383-411. *In* A Klute (ed.) Methods of  
590 Soil Analysis, Part 1. Physical and Mineralogical Methods. Agronomy Monograph No. 9  
591 (2ed). American Society of Agronomy/Soil Science Society of America, Madison, WI.

592 Gong, D., Shaozhong, K., Zhang, L., Taisheng, D., Limin, Y., 2006, A two-dimensional model of  
593 root water uptake for single apple trees and its verification with sap flow and soil water content  
594 measurements. Agricultural Water Management 83:119–129.

595 Green, S. R., Vogeler, I., Clothier, B. E., Mills, T. M., van den Dijssel, C., 2003a, Modelling water  
596 uptake by a mature apple tree. Australian Journal Of Soil Research, 41: 365-380.

597 Green, S.R. and Clothier, B.E. 1988, Water use of kiwifruit vines and apple trees by the heat-pulse  
598 technique. 1. Exp. Bot. 39: 115-123.

599 Green, S., Clothier, B., Jardine B., 2003b, Theory and Practical Application of Heat Pulse to  
600 Measure Sap Flow. Agronomy Journal; Nov/Dec 2003; 95, 6; ProQuest Agriculture Journals  
601 pg. 1371.

602 Hinnell, A.C., Ferré, T.P.A., Vrugt, J.A., Huisman, J.A., Moysey, S., Rings, J., Kowalsky, M.B.,  
603 2010, Improved extraction of hydrologic information from geophysical data through  
604 coupled hydrogeophysical inversion, Water Resour. Res., 46, W00D40,  
605 doi:10.1029/2008WR007060.

606 Jarvis, N.J., 1989, A simple empirical-model of root water-uptake. *J. Hydrol.* 107(1–4):57–72.  
607 doi:10.1016/0022-1694(89)90050-4.

608 Javaux M., Schroder T., Vanderborght, J. and Vereecken H., 2008, Use of a Three- Dimensional  
609 Detailed Modeling Approach for Predicting Root Water Uptake, *Vadose Zone Journal*, 7(3),  
610 1079 - 1088.

611 Jayawickreme H., Van Dam R., Hyndman D.W., 2008, Subsurface imaging of vegetation, climate,  
612 and root-zone moisture interactions. *Geophysical Research Letters*, VOL. 35, L18404.  
613 doi:10.1029/2008GL034690.

614 Jones, H. G., Tardieu, F., 1998, Modelling water relations of horticultural crops: a review. *Scientia*  
615 *Horticulturae* 74, 21-46.

616 Kaimal, J.C., Finnigan, J., 1994, *Atmospheric Boundary Layer Flows: Their Structure and*  
617 *Measurement*. Oxford University Press, New York, pp. 255–261

618 Kemna, A., Vanderborght, J., Kulesa, B., Vereecken, H., 2002, Imaging and characterisation of  
619 subsurface solute transport using electrical resistivity tomography ERT and equivalent  
620 transport models: *Journal of Hydrology*, 267, 125–146.

621 Koestel J., Kemna, A., Javaux, M., Binley A., and Vereecken, H., 2008, Quantitative imaging of  
622 solute transport in an unsaturated and undisturbed soil monolith with 3-D ERT and TDR,  
623 *Water Resour. Res.*, 44, W12411, doi:10.1029/2007WR006755.

624 Knight, B.P., Chaudri, A.M., McGrath, S.P., Giller, K.E., 1998, Determination of chemical  
625 availability of cadmium and zinc in soils using inert soil moisture samplers, *Environmental*  
626 *Pollution*, 99, 293-298.

627 Lin, H.J., Richards, D.R., Talbot, C.A., Yeh, G.-T., Cheng, J., Cheng, H., 1997. FEMWATER: a  
628 three-dimensional finite element computer model for simulating density-dependent flow and

629 transport in variably saturated media. US Army Corps of Engineers and Pennsylvania State  
630 University Technical Report CHL-97-12.

631 Manoli G., Bonetti, S., Domec, J.C., Putti, M., Katul G., and Marani, M., 2014, Tree root systems  
632 competing for soil moisture in a 3D soil-plant model, *Adv. Water Res.*, 66, 32-42, doi:  
633 10.1016/j.advwatres.2014.01.006.

634 Mauder, M. and Foken, T. 2004, Documentation and instruction manual of the eddy covariance  
635 software package TK2. Universität Bayreuth, Abt. Mikrometeorologie, Arbeitsergebnisse,  
636 <http://www.geo.unibayreuth.de/mikrometeorologie/ARBERG>, pp. 26-44.

637 Mauder, M., Oncley, S. P., Vogt, R., Weidinger, T., Ribeiro, L., Bernhofer, C., Foken, T., Kosiek,  
638 W., De Bruin, H. A. R. and Liu, H., 2007, The energy balance experiment EBEX-2000. Part II.  
639 Intercomparison of eddy-covariance sensors and post-field data processing methods. *Bound.-*  
640 *Layer Meteorol.* 123 doi:10.1007/s10546-006-9139-4.

641 Michot, D., Benderitter, Y., Dorigny, A., Nicoullaud, B., King, D., and Tabbagh, A., 2003, Spatial  
642 and temporal monitoring of soil water content with an irrigated corn crop cover using surface  
643 electrical resistivity tomography. *Water Resources Research*, vol. 39, no. 5, p. 1138.

644 Michot, D., Dorigny, A., Benderitter Y., 2001, Determination of water flow direction and corn  
645 roots-induced drying in an irrigated Beauce CALCISOL, using electrical resistivity  
646 measurements. *Comptes Rendus De L Academie Des Sciences Serie Ii Fascicule a-Sciences*  
647 *De La Terre Et Des Planetes* 332:29–36.

648 Musters, P.A.D., Bouten, W., 2000, A method for identifying optimum strategies of measuring soil  
649 water contents for calibrating a root water uptake model. *J. Hydrol*, 227:273-286.

650 Monego, M., Cassiani, G., Deiana, R., Putti, M., Passadore, G., and Altissimo, L.: Tracer test in a  
651 shallow heterogeneous aquifer monitored via time-lapse surface ERT, *Geophysics*, 75, WA61–  
652 WA73, doi:10.1190/1.3474601, 2010.

653 Motisi, A., Consoli S., Rossi F., Minacapilli M., Cammalleri C., Papa R., Rallo G., D'urso G.,  
654 2012, Eddy covariance and sap flow measurement of energy and mass exchange of woody  
655 crops in a Mediterranean environment. *Acta Horticulturae* 951, pp: 121-127.

656 Parasnis D.S., 1973, *Mining geophysics*, Elsevier Scientific Pub. Co., 395 pp.

657 Perri M.T., Cassiani, G., Gervasio, I., Deiana, R., Binley, A.M., 2012, A saline tracer test  
658 monitored via both surface and cross-borehole electrical resistivity tomography: comparison of  
659 time-lapse results, *Journal of Applied Geophysics*, 79, 6-16, doi:  
660 10.1016/j.jappgeo.2011.12.011.

661 Raats, P. A. C., 2007, Uptake of water from soils by plant roots. *Transp Porous Med* 68:5–28.

662 Rubin Y. and Hubbard S.S. (eds); 2005: *Hydrogeophysics*. Springer, Dordrecht, 523 pp.

663 Schneider, C. L., Attinger, S. , Delfs, J.-O., Hildebrandt, A., 2010, Implementing small scale  
664 processes at the soil-plant interface – the role of root architectures for calculating root water  
665 uptake profiles. *Hydrol. Earth Syst. Sci.*, 14, 279–289, 2010.

666 Shanahan P.W., A. Binley, W. R. Whalley, C.W. Watts, 2015, The use of electromagnetic  
667 induction to monitor changes in soil moisture profiles beneath different wheat genotypes, *Soil*  
668 *Sci. Soc. Am. J.*, 79: 459-466, doi: 10.2136/sssaj2014.09.0360.

669 Sheets K. R., Hendrickx J.M.H. (1995): Non invasive soil water content measurement using  
670 electromagnetic induction, *Water Resour. Res.*, 31, 2401– 2409.

671 Singha, K., and Gorelick, S.M., 2005, Saline tracer visualized with three dimensional electrical  
672 resistivity tomography: Field-scale spatial moment analysis, *Water Resour. Res.*, 41, W05023,  
673 doi:10.1029/2004WR003460.

674 Srayeddin, I., Doussan, C., 2009, Estimation of the spatial variability of root water uptake of maize  
675 and sorghum at the field scale by electrical resistivity tomography. *Plant Soil* 319:185–207.  
676 doi:10.1007/s11104-008-9860-5

677 Swanson, R.H. and Whitfield, D.W. 1981, A numerical analysis of heat pulse velocity theory and  
678 practice. *J. Exp. Bot.* 32:221-239.

679 Tye, A.M., Woung, S.D., Crout, N.M.J., Zhang, H., Preston, S., Barbosa-Jefferson, V.L., Davison,  
680 W., McGrath, S.P., Paton, G.I., Kilham, K., Resende, L., 2003, Predicting the activity of Cd<sup>2+</sup>  
681 and Zn<sup>2+</sup> in soil pore water from the radio-labile metal fraction, *Geochimica et Cosmochimica*  
682 *Acta*, 67(3), 375-385.

683 Ursino N., Cassiani, G., Deiana, R., Vignoli G., and Boaga, J., 2014, Measuring and Modelling  
684 water related soil – vegetation feedbacks in a fallow plot, *Hydrology and Earth System*  
685 *Sciences (HESS)*, doi:10.5194/hess-18-1105-2014.

686 Van Genuchten, M.T., 1980, A closed form equation for predicting the hydraulic conductivity of  
687 unsaturated soils. *Soil Sci. Soc. Am. J.* 44: 892–898

688 Vereecken H, Binley A, Cassiani G, Kharkhordin I, Revil A, Titov K. *Applied Hydrogeophysics*,  
689 Springer-Verlag, Berlin (eds), 2006.

690 Waxman M.H., Smits L.J.M., (1968): Electrical conductivities in oil-bearing shaly sands, *Soc. Petr.*  
691 *Eng. J.*, 8, 107–122.

692 Weill S., Altissimo M., Cassiani, G., Deiana, R., Marani, M. Putti, M., 2013, Saturated area  
693 dynamics and streamflow generation from coupled surface–subsurface simulations and field  
694 observations, *Advances in Water Resources*, 59, 196-208, doi:  
695 10.1016/j.advwatres.2013.06.007

696 Werban U, al Hagrey SA, Rabbel W., 2008, Monitoring of root-zone water content in the  
697 laboratory by 2D geoelectrical tomography. *Journal of Plant Nutrition and Soil Science*;  
698 171(6):927–935. doi: 10.1002/jpln.200700145. 781.

699 Wilson, K.B., Goldstein, A.H., Falge, E., 2002, Energy balance closure at FLUXNET sites.  
700 *Agriculture and Forest Meteorology*, 113, 223-243 Zimmermann E., Kemna A., Berwix J.,

701       Glaas W., Münch H.M. and Huisman J.A. 2008. A high-accuracy impedance  
702       spectrometer for measuring sediments with low polarizability. *Measurement Science and*  
703       *Technology* 19, 105603. doi:10.1088/0957-0233/19/10/105603.  
704

705

Acquisition #	Starting time	Ending time	Irrigation schedule	Date
0 (background)	10:40	11:00	11:30 to 16:30 4 l/h from each dripper	October 2, 2013
1	12:00	12:20		
2	13:00	13:20		
3	14:15	14:35		
4	15:00	15:20		
5	16:00	16:20		
6	17:00	17:20	7:00 to 12:00 4 l/h from each dripper	October 3, 2013
7	10:15	10:35		
8	11:05	11:25		
9	12:00	12:20		
10	13:00	13:20		
11	14:00	14:20		
12	15:00	15:20		
13	15:45	16:05		

706

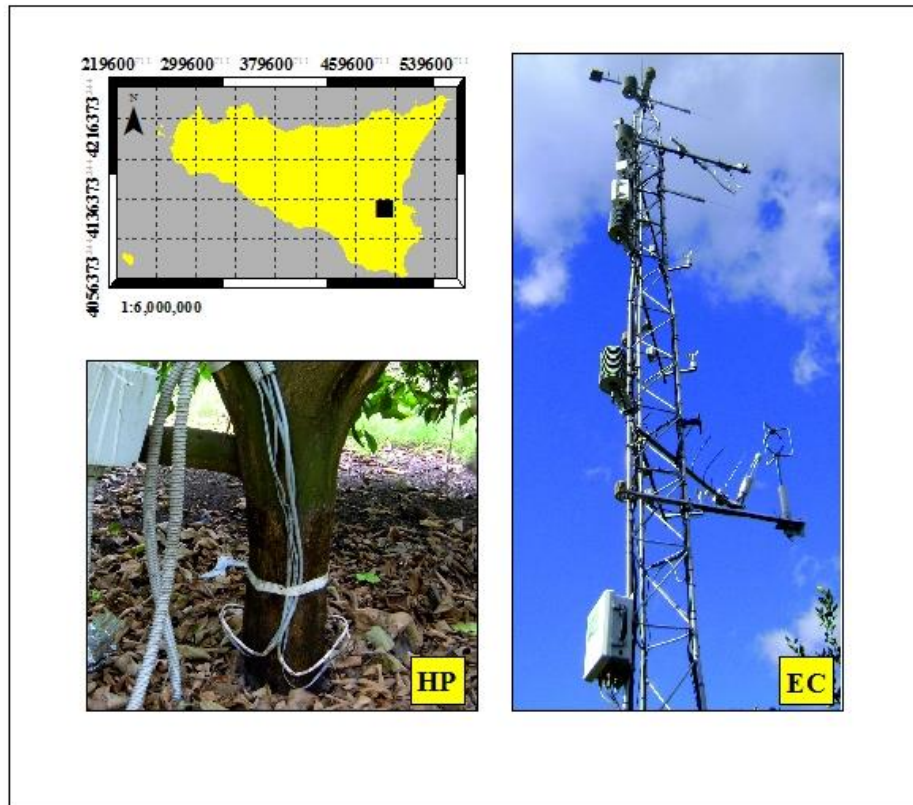
**Table 1:** times of acquisitions and irrigation schedule

707

708

709





710

711 **Figure 1:** Bulgherano experimental site: the Eddy Covariance (EC) tower and a Heat Pulse (HP)

712 Sap Flow installation on an orange tree.

713

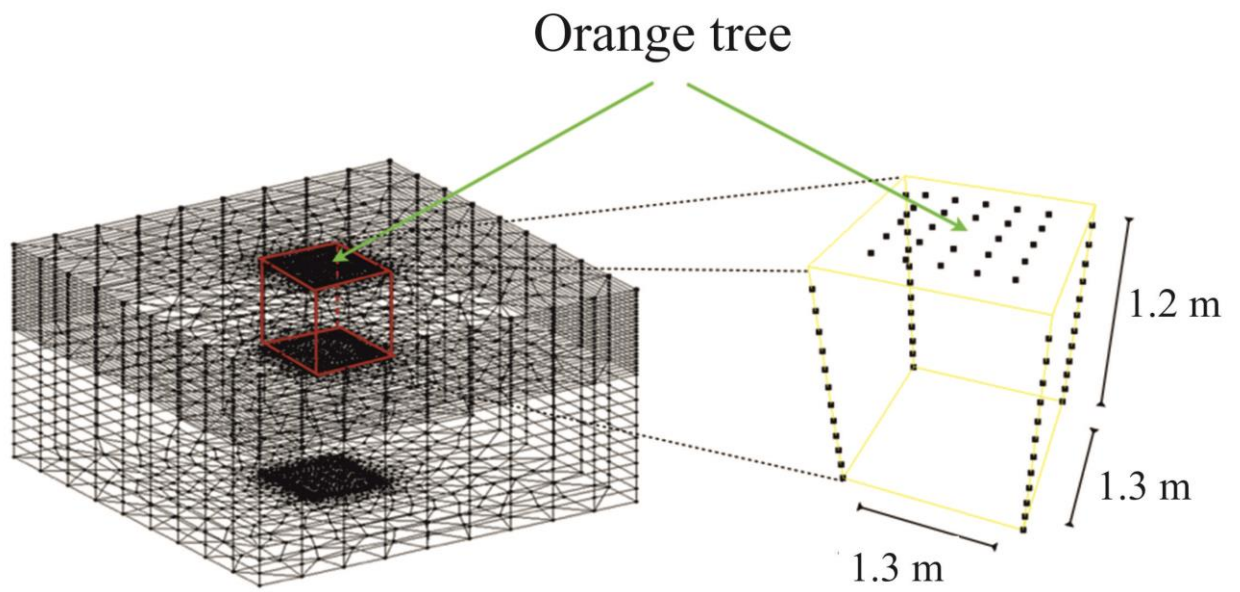
714



715

716 **Figure 2:** 3D ERT apparatus installed around one orange tree. The system is composed of four  
717 micro-boreholes carrying 12 electrodes each (see inset) and 24 surface electrodes – see text and  
718 Figure 3 for geometry details.

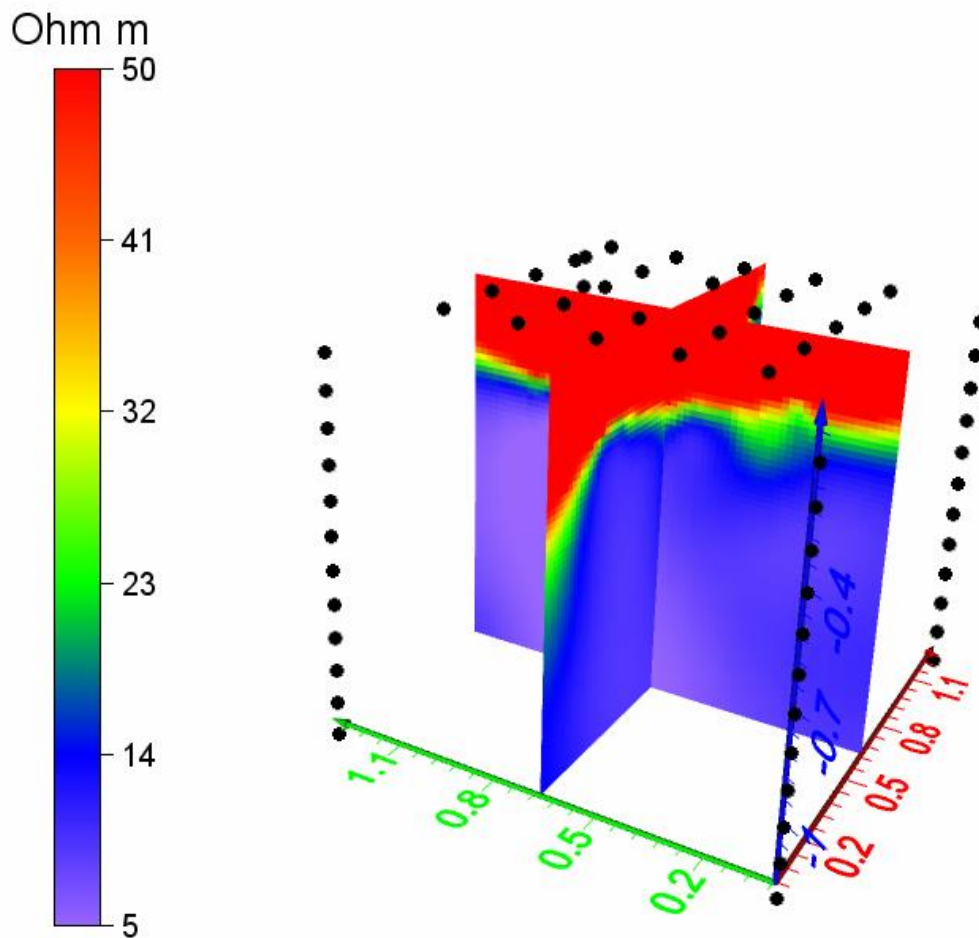
719



720

721 **Figure 3:** Electrode geometry around the orange tree and 3D mesh used for ERT inversion.

722



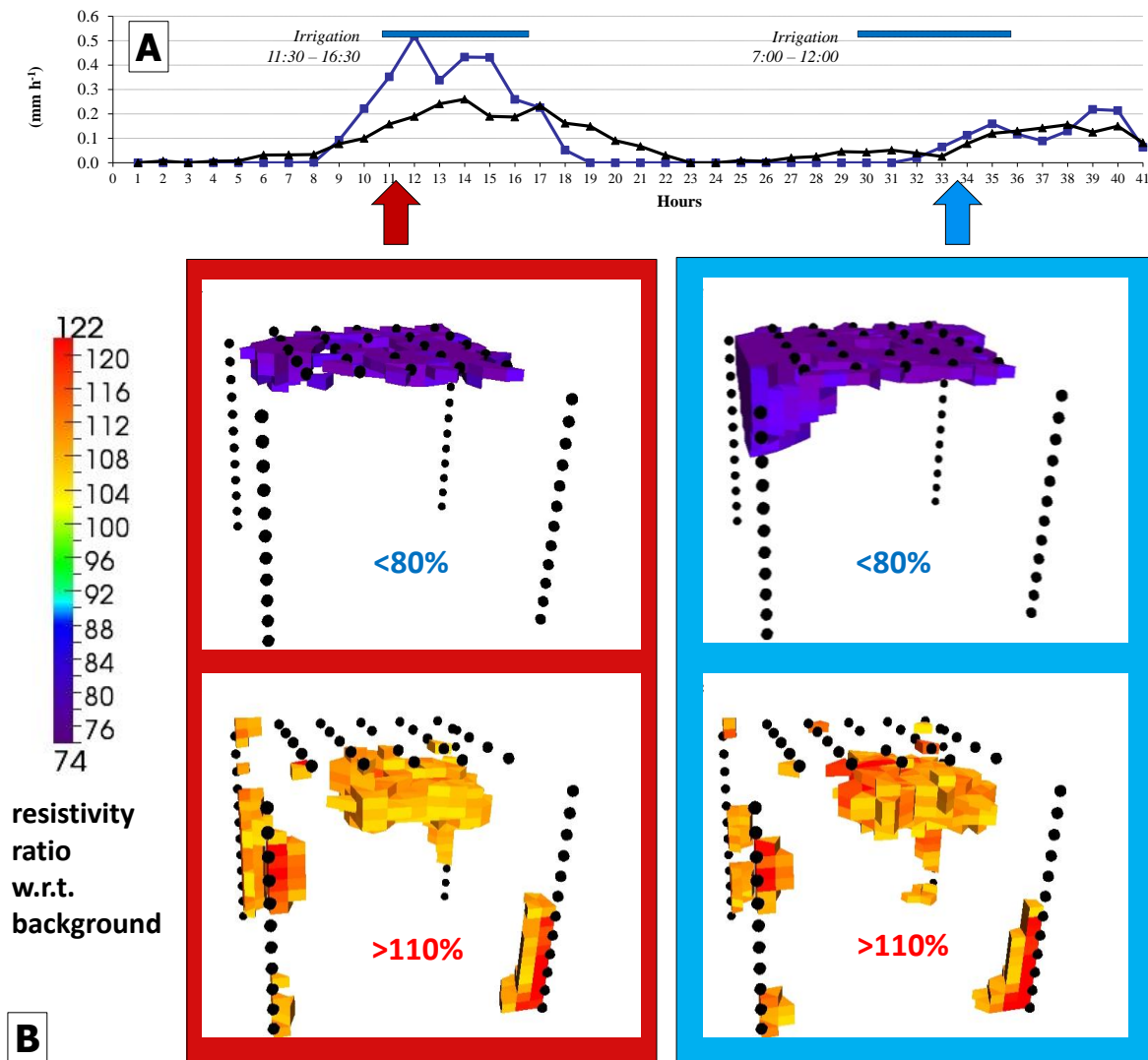
723

724 **Figure 4:** cross-sections of the ERT cube corresponding to the background acquisition of October  
 725 2, 2013, 11:00 a.m. Note the very strong difference in electrical resistivity between the top 40 cm  
 726 (above 50 Ohm) and the rest of the domain. The resistivity distribution is essentially one-  
 727 dimensional with depth, with very limited horizontal variations.

728

729

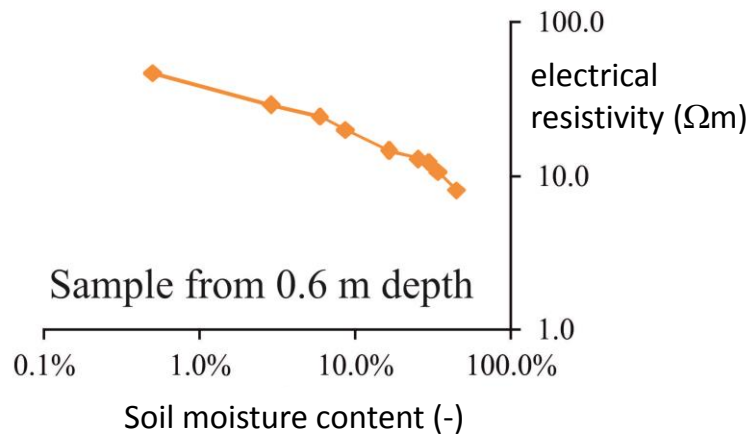
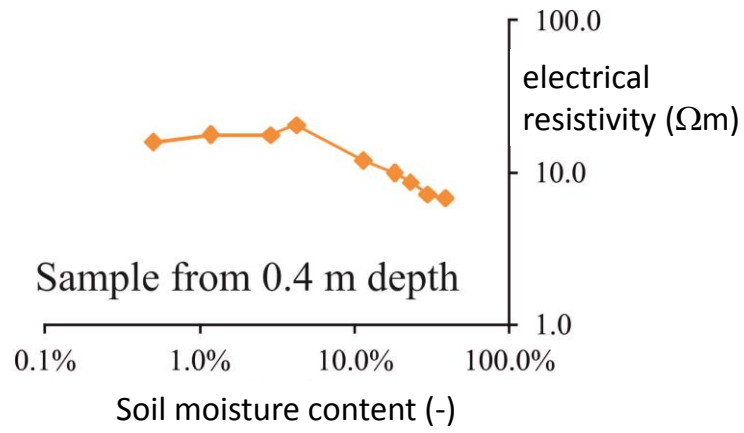
730



731

732 **Figure 5:** (A) time series of sap flow (black line) and EC-derived total evapotranspiration (blue  
 733 lines), both normalized in mm assuming an area of 20 m<sup>2</sup> pertaining to the orange tree monitored  
 734 with ERT. Time is given in hours from midnight of October 2. The two irrigation periods are  
 735 shown by the blue bars. (B) 3D ERT images of resistivity change with respect to background at  
 736 two selected time instants shown by the arrows in (A); the volumes corresponding to increase and  
 737 decrease of resistivity above and below certain thresholds (80% and 110%) are shown in separate  
 738 panels, for clarity.

739



740

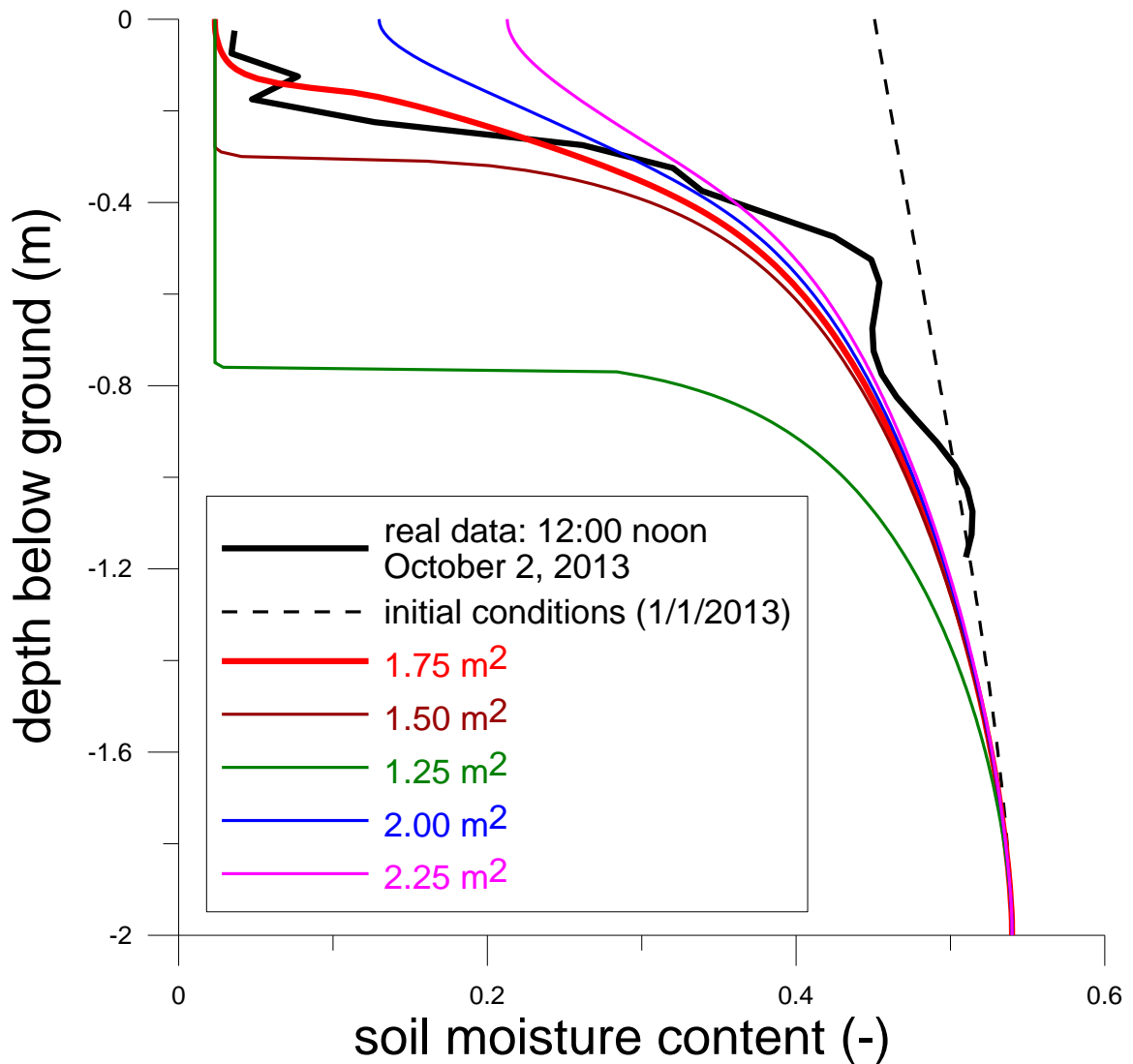
741 **Figure 6:** experimental relationships between resistivity and moisture content determined in the lab  
742 on samples taken at two different depths at the Bulgherano site, using water having the same  
743 electrical conductivity measured in the pore water in situ.

744

745

746

747



748

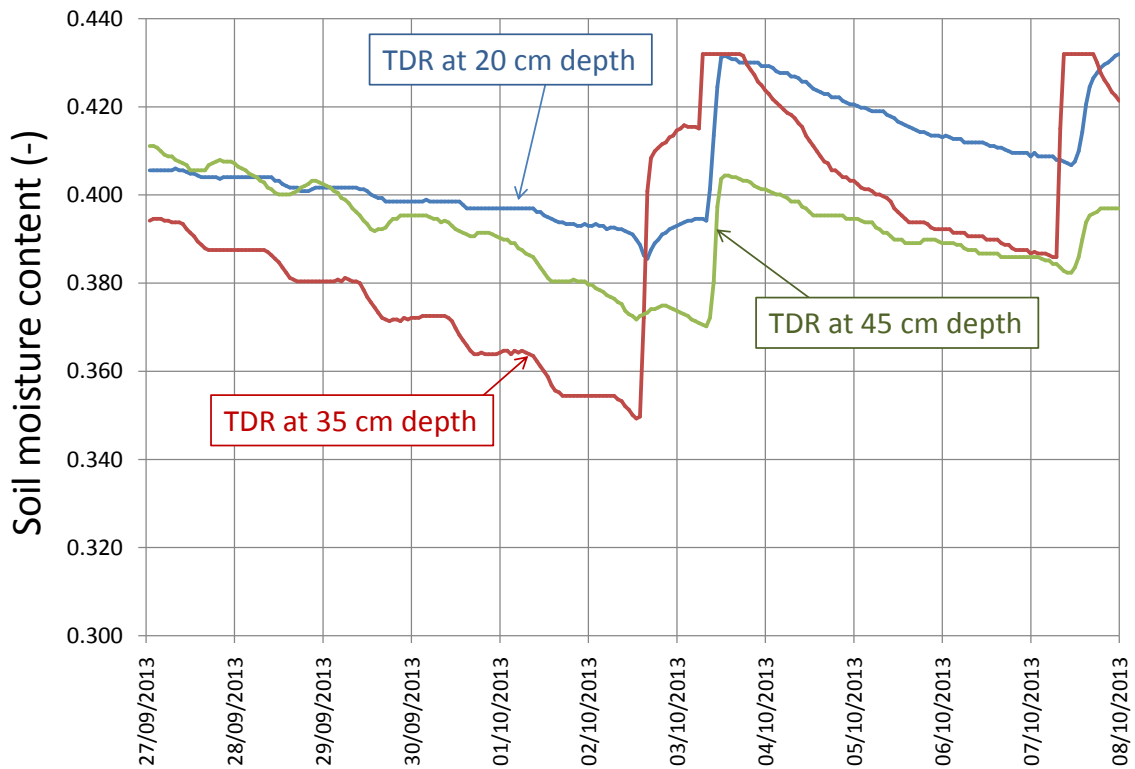
749 **Figure 7:** results of 1D Richards' equation simulations of the entire year 2013 till October 3, 11:00  
 750 a.m., i.e. in correspondence of the background ERT acquisition (the thick black line represents the  
 751 resulting estimated moisture content profile obtained from averaging horizontally the central  
 752 square meter of the ERT control volume). The different simulated curves correspond to different  
 753 assumed areas of root water uptake, and show how 1.75 m<sup>2</sup> is the area that allows to match the  
 754 observed real profile with good accuracy. Note also the high sensitivity of the results to the  
 755 estimated root uptake area.

756

757

758

759



760

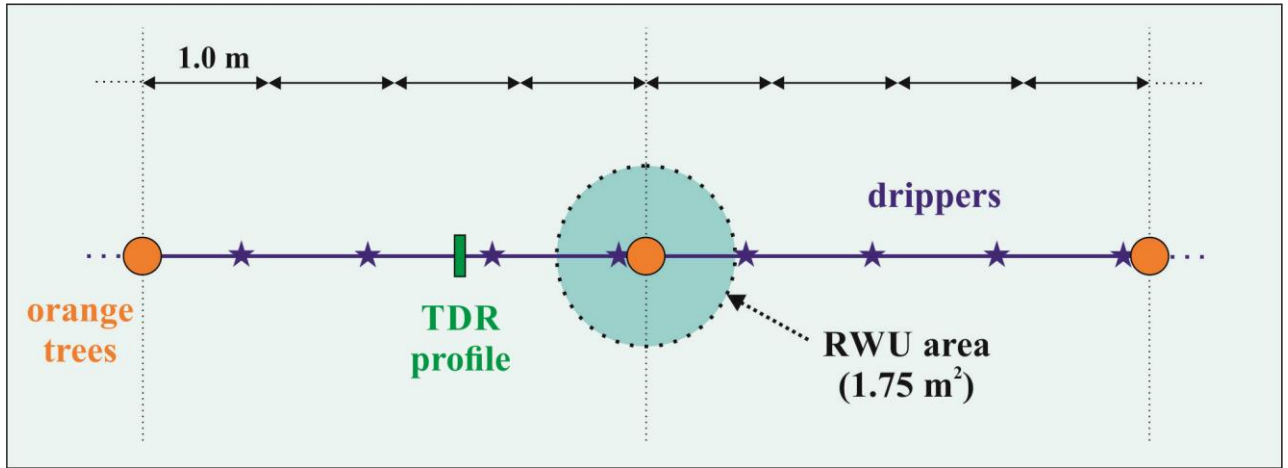
761 **Figure 8:** moisture content time series from three TDR probes located about 1.5 m from the ERT-  
762 monitored tree. The signal coming from the irrigation experiment of October 2, 2013 is very clear.

763 Before this experiment the system had been left without irrigation for about two weeks.

764

765





766

767 **Figure 9:** scheme of the experimental field with the location of the main sensors. The radius of the  
 768 root water uptake zone, assumed to be circular, is equal to about 0.75 m.

769

770